Frequency and resolution dependence of the anisotropic impedance estimation in cortical bone using time-resolved scanning acoustic microscopy

Kay Raum, Jan Reißhauer, Jörg Brandt
Department of Orthopedics, Q-BAM Group, Martin Luther University of Halle-Wittenberg, 06097 Halle, Germany

Received 9 February 2004; revised 17 June 2004; accepted 25 June 2004
Published online 8 October 2004 in Wiley InterScience (www.interscience.wiley.com). DOI: 10.1002/jbm.a.30156

Abstract: The influences of frequency and spatial resolution on the anisotropic impedance estimation of cortical bone was investigated in the frequency range 25–100 MHz. A set of spherically focused transducers provided a spatial resolution in the range from 150 down to about 20 μm. Four embedded cortical bone samples (two male, two female, two donors aged <30 years, two donors aged >70 years) were cut with different orientations relative to the long axis of the femur (0–90°). From each section, impedance maps were acquired in the C-scan mode. Histogram evaluations showed a similar angular dependence with a characteristic off-axis maximum of the estimated impedance for all samples and frequencies. The impedance values obtained with the 25-MHz transducer were significantly lower than those obtained with the 50- and 100-MHz transducers. Morphological parameters of the macrostructure, for example, size and distribution of the haversian channels and the resulting porosity, were estimated from the high-resolution acoustic images. These structures appeared to have a significant influence on the measured properties of the bone matrix for the low-frequency and low-aperture measurements. © 2004 Wiley Periodicals, Inc. J Biomed Mater Res 71A: 430–438, 2004

Key words: acoustic microscopy; anisotropy; bone; elastic properties; microstructure

INTRODUCTION

Bone is a heterogeneous and anisotropic material, which is composed of several levels of hierarchical organization. Ultrasonic inspection of cortical tissue has been established by Yoon and Katz[1–4], Ashman et al.,[5] and Van Buskirk et al.,[6] and the frequency range from 500 kHz to 2 MHz is now used extensively for the characterization of trabecular tissue.[7–15] In this frequency range, the wavelengths and acoustic beam dimensions are larger than the dimensions of the bone structure, for example, osteons or trabeculae. Therefore, bone has to be considered as a porous structure with greatly varying material properties, for which wave propagation is influenced by scattering, interference, and diffraction. Acoustical parameters, for example, speed of sound, broadband ultrasonic attenuation, and backscatter coefficient are affected by the structure, density, and elasticity of the individual components. Several theoretical concepts have been adapted or developed to model the ultrasound propagation in bone.[16] However, they require a large number of physical properties, which are usually not available. One potential way to assess these parameters is to increase the ultrasound frequency. Many studies were conducted at 50 MHz by Turner and colleagues. They measured the sound velocity in thin samples in pulse-echo mode. Significant differences were found between pre- and postmenopausal and osteoporotic iliac crest specimen of 40 Caucasian women.[17] Canine femoral bone specimens were measured at 10° increments from the long axis of the bone.[18] A significant anisotropy with an off-axis maximum at around 30° was observed. From a comparison of the anisotropic velocity of demineralized and decollagenized samples, it was concluded that the principal orientation of bone mineral was along the long axis of the femur whereas bone collagen was aligned at a 30° angle to it. Moreover, no significant differences were observed between cancellous and cortical bone.[19] Elastic parameters, for example, stiffness and Young's modulus, were calculated from the longitudinal sound velocities. However, macroscopic densities and Poisson ratios had to be used for the conversion.

Lees and Klopholz[20] observed dispersion in wet compact cow femora with unfocused ultrasound in the frequency range 5–100 MHz. At 70 MHz, they found a maximum of 3620 m/s in the direction perpendicular to the long axis of the femur and 4470 m/s

Correspondence to: K. Raum; e-mail: kay.raum@medizin.uni-halle.de
Contract grant sponsor: Deutsche Forschungsgemeinschaft; contract grant number: BR 1348/4-3

TABLE I
Pulse-Echo Beam Parameters

Manufacturer Model/Aperture	Panametrics V324/23[a]	Valpey Fisher V605/60[a]	KSI 100/60[a]
Center frequency[a]	25 MHz	50 MHz	100 MHz
Element size[a]	6 mm	6.35 mm	—
Radius of curvature[a]	15 mm	6.35 mm	—
f-number[a]	2.5	1	1.25
Time-of-flight (focus)	20.4 μs	17.0 μs[b]	3.97 μs
Pulse duration	119.0 ns	46.0 ns	101.0 ns
Center frequency	29.54 MHz	49.00 MHz	91.8 MHz
(peak/center)	28.95 MHz	44.95 MHz	92.5 MHz
$f_{1\ (-6\ dB)}$	21.90 MHz	26.00 MHz	84.4 MHz
$f_{2\ (-6\ dB)}$	36.00 MHz	63.90 MHz	100.7 MHz
Relative bandwidth	47.73%	77.35%	17.75%
(peak/center)	48.70%	84.31%	17.62%
Depth of focus	2100 μm	169 μm	139 μm
Confocal beam diameter	142 μm	23 μm	19.8 μm

[a]Parameters provided by the manufacturer.
[b]Including a 10-μs buffer rod.

parallel to it. At higher frequencies, the $V(z)$ technique was recently applied to determine surface acoustic wave velocities in trabecular bone.[21] Fourier analysis of the $V(z)$ curves revealed multiple peaks, which was explained by the occurrence of up to four different longitudinal and two Rayleigh wave velocities in individual measurements. The estimated velocities were in the range 2330–4330 m/s for the longitudinal waves and 1930–2070 m/s for the Rayleigh waves, respectively. Nevertheless, the large contributing surface area for this kind of measurement (approximately 2000 μm²) is still a limiting factor in terms of resolution and validity. Furthermore, these spot measurements make it difficult to assess the heterogeneous microstructure of bone tissue.

The alternative way is to scan the transducer in two dimensions across the surface of the sample. For low frequencies (e.g., 5 MHz), the spatial distribution of sound velocity can be assessed in thin sections of human femoral bone.[22] However, because of the limited resolution at this frequency, the sound velocity is affected by structural parameters, for example, pore size and porosity.

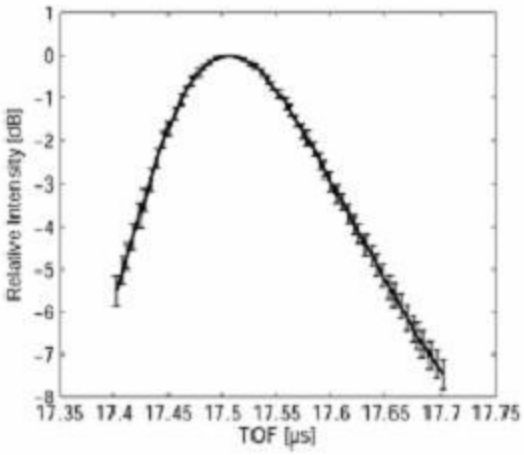

Figure 1. Time-of-flight (TOF) dependent defocus correction function for the V605 transducer (mean and standard deviation).

The spatial resolution is maximized, if the sample surface coincides with the focal plane of the transducer. For an infinite homogeneous half space the reflected amplitude is directly proportional to the reflection coefficient[23,24] and can be converted into a value of the acoustic impedance Z ($Z = \rho v_l$, where ρ is the mass density and v_l is the longitudinal sound velocity).[25–29] Significant correlations were found between acoustic impedance and density,[24] stiffness,[25,30] and bulk modulus[30] in the frequency range up to 50 MHz, and between impedance and Young's modulus at 900 MHz by comparison with nanoindentation results.[31] However, care must be taken when the structural dimensions of the tissue become comparable to the acoustic wavelength and the beam width, respectively. Nevertheless, quantitative acoustic impedance mapping in bone has been demonstrated for frequencies up to 900 MHz.[25–27,32–34] In this study, acoustic impedance distributions of cortical bone samples obtained with three focused transducers with operating frequencies up to 100 MHz were compared.

MATERIALS AND METHODS

Samples

Homogenous materials served as references for impedance calibration [TPX®, polystyrene, polycarbonate, polymethylmethacrylate (PMMA), Suprasil®, aluminum, titanium]. Speed of sound and mass density of these materials were determined by a low-frequency substitution method and by Archimedes' principle, respectively.

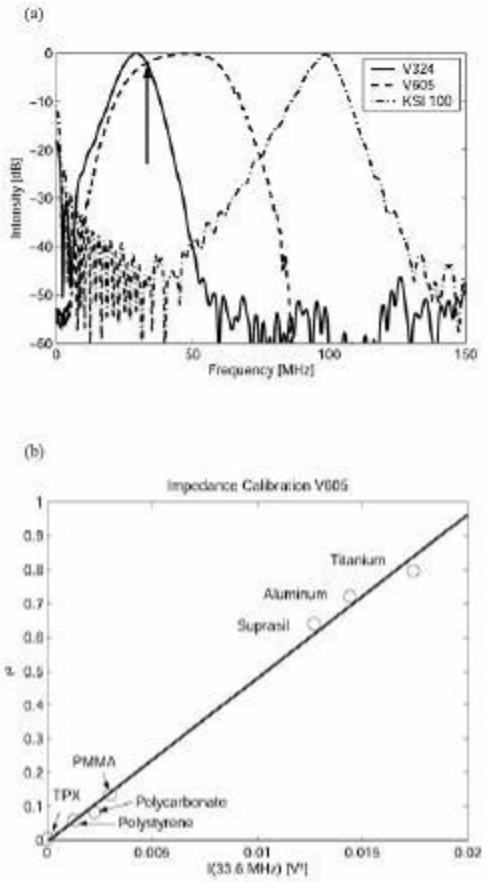

Figure 2. Power spectra of the transducers used (a). Monochromatic impedance distributions were calculated at the intercept frequency (arrow) of the V324 and V605 transducers. The confocal echo amplitudes of reference materials were used for the impedance calibration (b).

Four proximal cortical bone sections were obtained from human cadaver femora approximately 10 cm beneath the femoral head. For each gender, samples from one young and one senium donor without bone pathologies in history were chosen for the investigation. The samples were cut with various angles (0°, 10°, 15°, 30°, 45°, 60°, and 90°) relative to the femoral long axis using a diamond saw (Exakt—Trennschleifsystem Makro; Exakt Apparatebau, Norderstedt, Germany). After dehydration and embedding in PMMA, flat surfaces were prepared by a grinding procedure with successively decreasing grain size (1200, 2400, 4000; Exakt-Mikroschleif system, Exakt Apparatebau).

The experimental setup was confirmed by the Ethic Commission of the Martin Luther University.

Experimental setup

A custom scanning acoustic microscope was used. It consists of a three-axis high-precision scanning stage, a 200-MHz pulser/receiver (Panametrics 5900PR, Waltham, MA), and a 500 MS/s A/D-card (Gage 8500). All components are controlled by a custom software (SAMEx; Q-BAM, Halle, Germany). A set of spherically focused transducers (V324/23°: Panametrics; V605/60°: Valpey Fisher, Hopkinton, MA; KSI 100/60°: KSI, Herborn, Germany) provided spatial resolutions in the range from 150 down to about 20 μm. The pulse-echo sound field characteristics were determined by the wire technique[35] and are summarized in Table I.

The samples were completely immersed in a temperature-controlled tank filled with distilled, degassed water at 25°C. The sample surfaces were placed in the focal plane of the transducer and C-scans were acquired, whereas for each scanned point, the entire pulse-echo signal was stored.

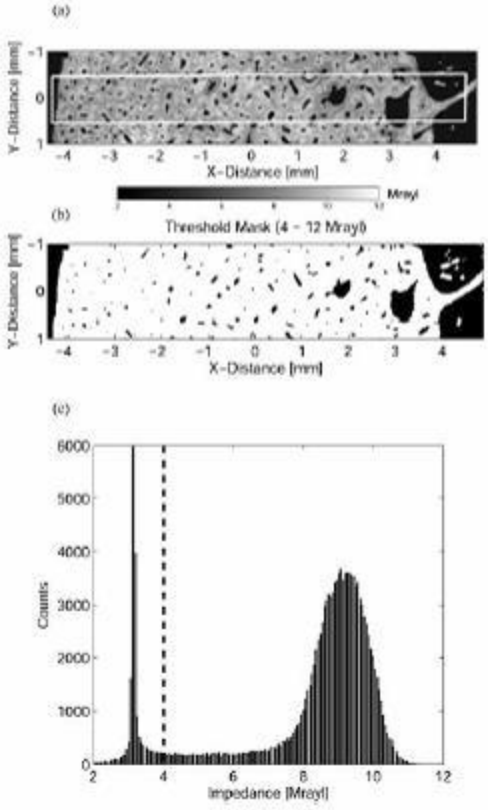

Figure 3. Impedance map with ROI selection (a), threshold mask (b), and histogram (c) of the selected region. The regions filled with the embedding material (narrow peak at 3 Mrayl) were excluded from the analysis using the threshold mask.

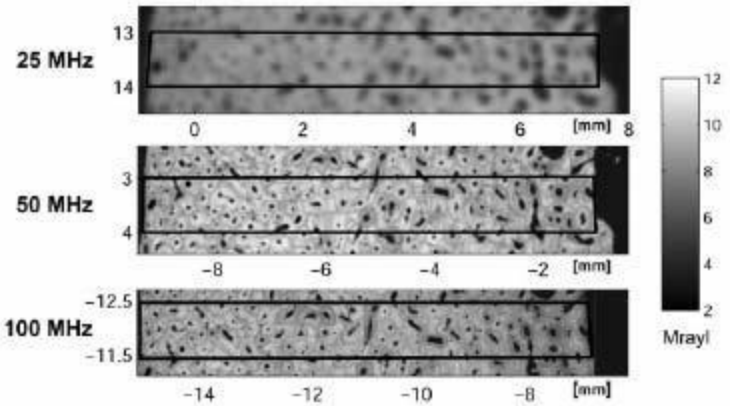

Figure 4. Broadband impedance maps of the 0° cut of the young male sample. The ROIs for histogram evaluation are indicated with black lines.

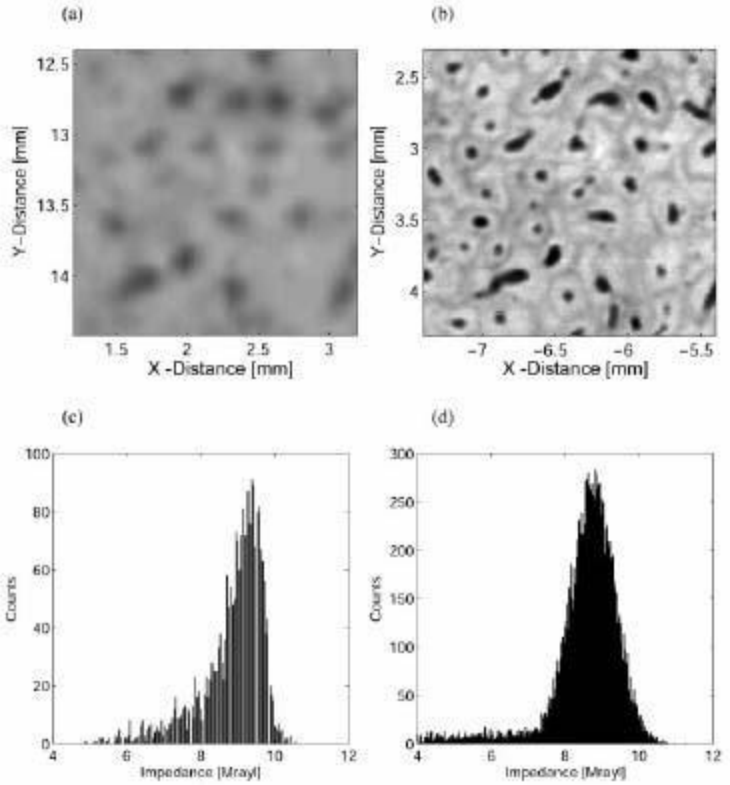

Figure 5. Monochromatic 33.6-MHz impedance maps measured with the V324 (a) and V605 (b) transducers. The corresponding histograms are drawn below (c) and (d).

TABLE II
Regression Coefficients for $Z_{median} = A + B \cdot Z_{mean}$

	A	B	R
$V324_{bb}$ (25 MHz)	−0.8759	1.1449	0.99365
$V324_{mc}$ (33.6 MHz)	−1.12165	1.1653	0.99366
$V605_{mc}$ (33.6 MHz)	−0.38445	1.0673	0.99668
$V605_{bb}$ (50 MHz)	−0.21073	1.0455	0.99764
KSI 100/60°$_{bb}$ (100 MHz)	−0.20617	1.0371	0.99853

Impedance calibration and evaluation

For all reference materials, the pulse-echo signal was measured as a function of the sample-transducer distance. All signals were band-pass filtered (V324: 5–70 MHz; V605: 5–90 MHz; KSI 100/60°: 5–200 MHz) using a zero-phase filter function. After conversion to decibel (0 dB corresponds to the confocal echo amplitude), time-of-flight dependent defocus corrections were estimated from the characteristic $V(z)$ curve of each transducer (Fig. 1).

The confocal echo amplitudes of the reference materials were used for impedance calibration in two different ways: broadband impedances were estimated using the amplitudes of the Hilbert-transformed (envelope) signals, and monochromatic impedances were determined from the 33.6-MHz components of the power spectra for the V324 and V605 transducers (Fig. 2).

The same processing (band-pass filter, Hilbert-transformation) was applied to the C-scan data. After defocus correction, the echo amplitudes were converted into values of the acoustic impedance. Histogram evaluations were performed on identical stripes of 1-mm width (peripheral to central; Fig. 3) for each measurement. Regions filled with the embedding material, for example, in the haversian channels were excluded from the evaluation using a 4-Mrayl threshold mask. The histograms were normalized in order to compensate for different amounts of data for the individual scans.

Porosity (P; ratio between cavity area and cortical area) and cavity density (CD; number of cavities per mm^2) were assessed from the exclusion maps.

RESULTS

Reproducibility

All reference materials were measured at least 10 times at different days. The maximum relative standard error of the estimated mean impedances was 0.42%.

Resolution

Figure 4 shows the impedance maps of the 0° cut of the young male donor. At 25 MHz, the haversian channels are not completely resolved whereas, at the higher frequencies, the channels as well as the boundaries between osteons and secondary osteons can be distinguished.

Monochromatic impedance maps obtained with the V324 and the V605 transducers are shown in Figure 5. Resolution differences in these images are directly linked to the numerical aperture of the used transducers. The histogram of the V324 measurement is clearly asymmetric and shifted toward lower impedance values. This shift was quantitatively assessed by linear regression between the means and medians of all distributions. Only for the low frequencies and low-aperture measurements the slope of the regression remarkably deviates from one (Table II).

Moreover, the 25-MHz-broadband mean, median, and standard deviation values were lower compared with the other measurements.

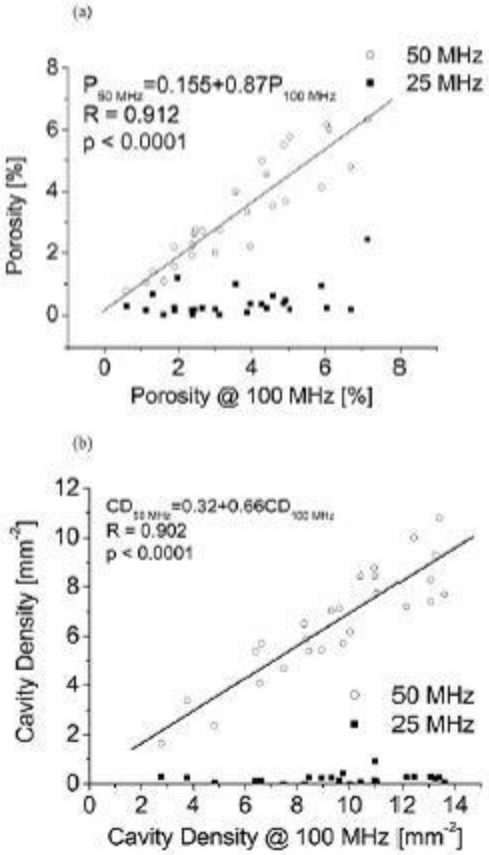

Figure 6. Estimated P and CD for the different measurements. With the 25-MHz transducer morphological parameters cannot be derived.

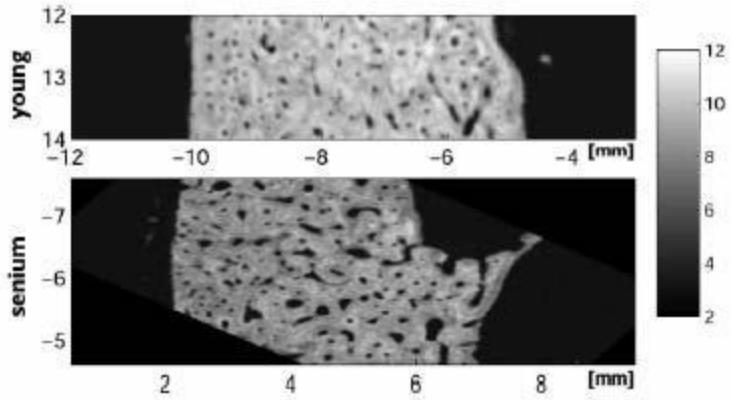

Figure 7. The 50-MHz broadband impedance maps of a 0° cut of the young and the senium female donors.

Morphology

Morphological parameters were compared for the 0–30° cuts. The estimation failed for the V324 measurements. The CD and P values were slightly higher for the 100-MHz transducer compared with the 50-MHz transducer. However, the values were highly correlated (Fig. 6).

Differences in the morphology can be particularly seen between the young female and the other samples (Fig. 7). Both channel density and porosity were lower in the young samples (Table III).

Impedance versus frequency

After merging the broadband histograms into the three frequency groups, an increase of the mean impedance with increasing frequency was observed. Student t tests showed significant differences between 25 MHz and the higher frequencies (50 MHz: $p = 0.0040$, 100 MHz: $p = 0.0001$). The same trend was found for the individual samples. However, the differences were only significant for the senium samples between 25 and 100 MHz (Fig. 8 and Table IV).

Significant differences between the samples were observed at 50 and 100 MHz. At 50 MHz, the mean impedance of the female senium donor was lower compared with impedances of both male donors. At 100 MHz, the decrease was only significant compared with the senium samples. It should be noted that the standard deviations of the impedance distributions are smaller in the senium samples compared with the young samples at the 100-MHz measurement, whereas this trend was reversed in the 25-MHz data.

TABLE III
Channel Density and Porosity (Mean and Standard Deviation) for the 0°–30° Cuts Measured at 100 MHz

	CD ($1/mm^2$)	Porosity (%)
Male (73)	12.59 ± 1.08	5.16 ± 1.77
Male (25)	11.23 ± 1.75	3.69 ± 0.70*
Female (76)	12.64 ± 1.25	5.38 ± 0.87
Female (20)	7.55 ± 1.25*	2.16 ± 0.25*

*Significant gender-specific age differences.

Anisotropy

Similar anisotropic impedance distributions were observed for all samples and all frequencies. To explore the complex relations between loading angle, impedance distribution, and frequency, the normal-

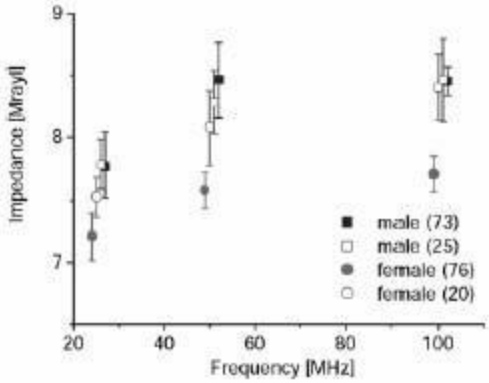

Figure 8. Mean and standard deviation of the broadband impedances of all samples as a function of frequency.

TABLE IV
Mean and Standard Error of the Acoustic Impedance After Merging the Normalized Histograms of All Angles

	25 MHz	50 MHz	100 MHz
Male (73)	7.78 ± 0.26	8.46 ± 0.31	8.45 ± 0.11
Male (25)	7.79 ± 0.19	8.28 ± 0.25	8.46 ± 0.34
Female (76)	7.21 ± 0.20	7.58 ± 0.15	7.71 ± 0.15
Female (20)	7.53 ± 0.16	8.08 ± 0.29	8.41 ± 0.27

ized angular-dependent histograms are presented as color-coded contour plots for each frequency in Figure 9. The lowest peak values of the histograms always occurred at 90° (relative to the long axis of the femur). The most regular pattern was observed at 100 MHz. At this frequency, the histograms for all angles have a symmetric shape. Width and peak values, however, varied considerably. The narrowest distributions can be seen at 10° and 45°. Between these two angles, the distributions are broadened and the peak reaches a local maximum. The highest peak value can be seen at 0°. The contour plots of the lower frequencies have a similar shape. In addition to the more irregular pattern, an impedance downshift is apparent particularly in the 25-MHz plot.

An anisotropy ratio was defined as the ratio between the maximum peak value to the peak value at 90°. The highest anisotropy was observed at 50 MHz (anisotropy ratio = 1.32). For the 25- and 100-MHz measurements, the anisotropy ratios were 1.23 and 1.15, respectively.

Influence of morphology on impedance estimation

Multiple regression was performed between cavity density and porosity and the relative decrease of the 25- and 50-MHz impedance estimations (compared with the 100-MHz results). Both parameters had significant influences on the impedance decrease (25 MHz: $R^2 = 0.87$, $p = 0.037$, $\beta_{CD} = 0.798$, $\beta_P = 0.138$; 50 MHz: $R^2 = 0.80$, $p = 0.042$, $\beta_{CD} = 0.794$, $\beta_P = 0.104$).

DISCUSSION

Information about the elastic properties of the cortical microstructure was obtained with all transducers. However, the resolution of the 25-MHz transducer was not sufficient to separate the haversian channels from the bone matrix. The resulting artifact in the acoustic impedance estimation of the bone matrix is dependent on number, size, distribution, and content of the channels. Monochromatic impedance estimations allowed quantification of the influences of frequency and numerical aperture separately. The results indicate the requirement of a high aperture in addition to a high frequency for a reliable discrimination between matrix and channels. The resolution limit of the 50- and 100-MHz transducers is in the range of the smallest occurring haversian channels in human cortical bone. Therefore, the channels are usually resolved and can be separated from the bone matrix. This in turn allowed quantitative assessment of morphologically relevant parameters in addition to information about the elastic properties of the matrix. The estimated CD and P values are in the range of histomorphometric values reported by Wachter et al.[36,37] However, a direct comparison was not possible, because these structural parameters are known to vary considerably even within a single femur at different anatomical locations.[22] Moreover, the different values obtained at 50 and 100 MHz suggest a remaining dependence of the estimated values on the selection of the impedance threshold level. The value used in this study (4 Mrayl) presumably failed to exclude the smallest channels and led to slightly reduced channel size estimations. These effects need to be further optimized.

Anisotropy of the bone matrix was observed for all frequencies. The angular dependence is consistent with macroscopic anisotropic Young's modulus data assessed with low-frequency ultrasound,[38,39] high-frequency sound velocity measurements at 50 MHz by Turner et al.,[18] and the anisotropic microscopic impedance observed at 900 MHz by Smitmans et al.[34] Insuf-

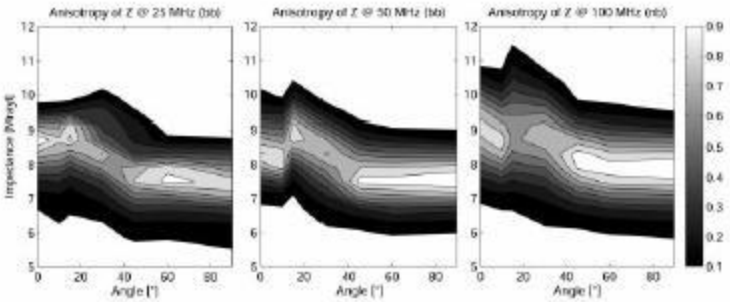

Figure 9. Contour plots of the impedance histograms as a function of the loading angle.

ficient resolution again limits the reliability of the observations at low frequencies or low transducer apertures. The current results suggest that artifacts resulting from the presence of cavities in human cortical bone cannot be neglected, if the lateral resolution is worse than approximately 20 µm. For the 100-MHz/60° transducer, these artifacts appear to be minimized. However, no significant differences were found between the 50- and 100-MHz measurements. Approximately 90% of the impedance decrease at lower frequencies can be explained by structural parameters. A remaining factor might be caused by dispersion, which would support the observations of Lees and Klopholz,[20] and considerably reduced impedance values found at 900 MHz.[34]

A drawback of the high-frequency measurements is the limited depth of focus. Careful sample preparation and alignment as well as stable measurement conditions and a robust defocus correction are necessary for a reliable impedance estimation. The uncertainty of the correction depends on the relative distance of the measured reflection from the focus toward the end of the depth of focus (see Fig. 1). Therefore, defocus correction errors become more severe at higher frequencies.

A limitation of this study is the use of plane samples. This setup limits the number of observation angles and the information is obtained from different anatomical sites. Although it has been shown that two-dimensional impedance mapping allows assessment of the anisotropy of the cortical bone matrix separately from the haversian channels, new sample preparation and measurement concepts need to be developed in order to obtain this information from a smaller sample volume.

Although a comprehensive investigation of age- and gender-specific differences of the cortical microstructure was beyond the scope of this study, the results demonstrate that high-resolution acoustic microscopy is sensitive to variations of both structural and anisotropic elastic properties of the cortical bone microstructure.

References

1. Yoon HS, Katz JL. Ultrasonic wave propagation in human cortical bone. I. Theoretical considerations for hexagonal symmetry. J Biomech 1976;9:407–412.
2. Yoon HS, Katz JL. Ultrasonic wave propagation in human cortical bone. II. Measurements of elastic properties and microhardness. J Biomech 1976;9:459–464.
3. Yoon HS, Katz JL. Ultrasonic wave propagation in human cortical bone. III. Piezoelectric contribution. J Biomech 1976;9:537–540.
4. Yoon HS, Katz JL. Ultrasonic properties and microtexture of human cortical bone. Ultrason Tissue Charact II 1979;189–196.
5. Ashman RB, Cowin SC, Rho JY, Van Buskirk WC, Rice JC. A continuous wave technique for the measurement of the elastic properties of cortical bone. J Biomech 1984;17:349–361.
6. Van Buskirk WC, Cowin SC, Ward RN. Ultrasonic measurement of orthotropic elastic constants of bovine femoral bone. J Biomech Eng 1981;103:67–72.
7. Bouxsein ML, Radloff SE. Quantitative ultrasound of the calcaneus reflects the mechanical properties of calcaneal trabecular bone. J Bone Miner Res 1997;12:839–846.
8. Chaffai S, Peyrin F, Nuzzo S, Porcher R, Berger G, Laugier P. Ultrasonic characterization of human cancellous bone using transmission and backscatter measurements: relationships to density and microstructure. Bone 2002;30:229–237.
9. Chappard C, Laugier P, Fournier B, Roux C, Berger G. Assessment of the relationship between broadband ultrasound attenuation and bone mineral density at the calcaneus using BUA imaging and DXA. Osteoporos Int 1997;7:316–322.
10. Gluer CC, Barkmann R, Heller M. Quantitative ultrasound. State of the art 1999. Radiologe 1999;39:213–221.
11. Han S, Rho JY, Medige J, Ziv I. Ultrasound velocity and broadband attenuation over a wide range of bone mineral density. Osteoporos Int 1996;6:291–296.
12. Han SM, Rho JY. Dependence of broadband ultrasound attenuation on the elastic anisotropy of trabecular bone. Proc Inst Mech Eng 1998;212:223–227.
13. Hans D, Wu C, Njeh CF, Zhao S, Augat P, Newitt D, Link T, Lu Y, Majumdar S, Genant HK. Ultrasound velocity of trabecular cubes reflects mainly bone density and elasticity. Calcif Tissue Int 1999;64:18–23.
14. Laugier P, Droin P, Laval-Jeantet AM, Berger G. *In vitro* assessment of the relationship between acoustic properties and bone mass density of the calcaneus by comparison of ultrasound parametric imaging and quantitative computed tomography. Bone 1997;20:157–165.
15. Wear KA. Anisotropy of ultrasonic backscatter and attenuation from human calcaneus: implications for relative roles of absorption and scattering in determining attenuation. J Acoust Soc Am 2000;107:3474–3479.
16. Hughes ER, Leighton TG, Petley GW, White PR. Ultrasonic propagation in cancellous bone: a new stratified model. Ultrasound Med Biol 1999;25:811–821.
17. Hasegawa K, Turner CH, Recker RR, Wu E, Burr DB. Elastic properties of osteoporotic bone measured by scanning acoustic microscopy. Bone 1995;16:85–90.
18. Turner CH, Chandran A, Pidaparti RM. The anisotropy of osteonal bone and its ultrastructural implications. Bone 1995;17:85–89.
19. Turner CH, Rho JY, Takano Y, Tsui TY, Pharr GM. The elastic properties of trabecular and cortical bone tissues are similar: results from two microscopic measurement techniques. J Biomech 1999;32:437–441.
20. Lees S, Klopholz DZ. Sonic velocity and attenuation in wet compact cow femur for the frequency range 5 to 100 MHz. Ultrasound Med Biol 1992;18:303–308.
21. Jorgensen CS, Kundu T. Measurement of material elastic constants of trabecular bone: a micromechanical analytic study using a 1 GHz acoustic microscope. J Orthop Res 2002;20:151–158.
22. Bensamoun S, Ho Ba Tho MC, Luu S, Gherbezza JM, Belleval JF. Spatial distribution of acoustic and elastic properties of human femoral cortical bone. J Biomech 2004;37:503–510.
23. Hirsekorn S, Pangraz S, Weides G, Arnold W. Measurement of elastic impedance with high spatial resolution using acoustic microscopy. Appl Phys Lett 1995;67:745–747.
24. Hirsekorn S, Pangraz S, Weides G, Arnold W. Erratum: measurement of elastic impedance with high spatial resolution using acoustic microscopy. Appl Phys Lett 1996;69:2138.
25. Mounier A, Riot O, Christol P, Katz JL. Characterization of local anisotropic elastic properties of femoral and tibial diaphysis using acoustic transmission measurements and acoustic microscopy. In: Middleton TJ, Palotti G, editors. Interfaces in

medicine and mechanics. II. London: Elsevier Applied Science; 1991. p 454–63.
26. Raum K, Jenderka KV, Klemenz A, Brandt J. Multi layer analysis: quantitative scanning acoustic microscopy for tissue characterization at a microscopic scale. IEEE Trans Ultrason Ferroelect Freq Contr 2003;50:507–516.
27. Raum K. Ultrasonic characterization of hard tissues. In: Kundu T, editor. Ultrasonic nondestructive evaluation: engineering and biological material characterization. Boca Raton, FL: CRC Press; 2003. p 761–781.
28. Shieh SJ, Zimmerman MC, Langrana NA. The application of scanning acoustic microscopy in a bone remodeling study. J Biomech Eng 1995;117:286–292.
29. Zimmerman MC, Prabhakar A, Chokshi BV, Budhwani N, Berndt H. The acoustic properties of normal and imbedded bovine bone as measured by acoustic microscopy. J Biomed Mater Res 1994;28:931–938.
30. Raum K, Brandt J. Simultaneous determination of acoustic impedance, longitudinal and lateral wave velocities for the characterization of the elastic microstructure of cortical bone. In: Proceedings of the 5th world congress of ultrasound, 7 Sept–10 Sept, Paris: SFA; 2003. p 321–324.
31. Brandt J, Raum K, Klemenz A, Seidler S. Micromechanics of bone: comparative measurement with scanning acoustic microscopy and nanoindentation. In: Proceedings of the IEEE ultrasonics symposium, 5 Oct–8 Oct, Honolulu: IEEE; 2003. p 22.
32. Eckardt I, Hein HJ. Quantitative measurements of the mechanical properties of human bone tissues by scanning acoustic microscopy. Ann Biomed Eng 2001;29:1043–1047.
33. Katz JL, Meunier A. Scanning acoustic microscopy of human and canine cortical bone microstructure at high frequencies. Stud Health Technol Inform 1997;40:123–137.
34. Smitmans L, Raum K, Brandt J, Klemenz A. Variations in the microstructural acousto-mechanical properties of cortical bone revealed by a quantitative acoustic microscopy study. In: Proceedings of the IEEE ultrasonics symposium, 22 Oct–25 Oct, San Juan, Puerto Rico: IEEE; 2001. p 1379–1382.
35. Raum K, O'Brien WD. Pulse-echo field distribution measurement technique for high-frequency ultrasound sources. IEEE Trans Ultrason Ferroelect Freq Contr 1997;44:810–815.
36. Wachter NJ, Augat P, Krischak GD, Mentzel M, Kinzl L, Claes L. Prediction of cortical bone porosity *in vitro* by microcomputed tomography. Calcif Tissue Int 2001;68:28–42.
37. Wachter NJ, Krischak GD, Mentzel M, Sarkar MR, Ebinger T, Kinzl L, Claes L, Augat P. Correlation of bone mineral density with strength and microstructural parameters of cortical bone *in vitro*. Bone 2002;31:90–95.
38. Katz JL, Yoon HS, Lipson SF, Maharidge R, Meunier A, Christel P. The effects of remodeling on the elastic properties of bone. Calcif Tissue Int 1984;36:31–36.
39. Katz JL, Meunier A. The elastic anisotropy of bone. J Biomech 1987;20:1063–1070.